Theoretical Model of Exciton States and Ultra-fast Energy Transfer in Heliobacterial Type-I Homodimeric Reaction Center

Akihiro Kimura* and Shigeru Itoh

Department of Physics, Graduate School of Science, Nagoya University, Nagoya, Japan

E-mail: akimura@tb.phys.nagoya-u.ac.jp

Phone: +81-52-789-2873

Abstract

A simple theoretical model of exciton dynamics was proposed to interpret the fast excitation energy transfer process in the Type-I homodimeric reaction center of *Heliobacterium modesticaldum* (hRC); this structure was recently identified and shown to resemble that of the plant/cyanobacterial photosystem I (PSI) reaction center. The exciton state model, which mainly relies on the geometries of 54 bacteriochlorophyll (BChl) g, 4 BChl-g' and 2 chlorophyll (Chl) a on hRC and assumes constant site energy values for the pigments, reproduced the absorption spectrum of hRC rather well. The model also enabled numerical analysis of the exciton dynamics on hRC, which can be compared with the decay-associated spectra obtained by the laser spectroscopy experiments. The model indicates that the stronger transition-dipole moment on BChl-g contributes to the faster energy transfer due to the higher coherency of the delocalized exciton states on hRC compared to that on PSI that arranges Chl-a at almost homologous locations.

Introduction

The initial process of photosynthesis starts with the excitation energy transfer (EET) from the light-excited antenna pigments to the special pairs of chlorophylls (Chls), or monomeric Chls associated with the special pairs, to promote the charge separation in the reaction center (RC) on the membranes. This is followed by sequential electron transfer reactions to convert light energy into biochemical energy. Experimental and theoretical studies have indicated the highly optimized nature of the elementary processes on different RC structures in a variety of photosynthetic organisms from higher plants to anoxygenic bacteria.[1–9]

Two types of RCs, photosystem I and II (PSI and PSII), are known to function in a series in plant/cyanobacterial oxygenic photosynthesis.[10,11] On the other hand, only one type of RC functions in the photosynthesis of bacteria. Purple photosynthetic bacteria use only Type-II RCs that have structures homologous the central cores of to PSII. Structures of RCs of green

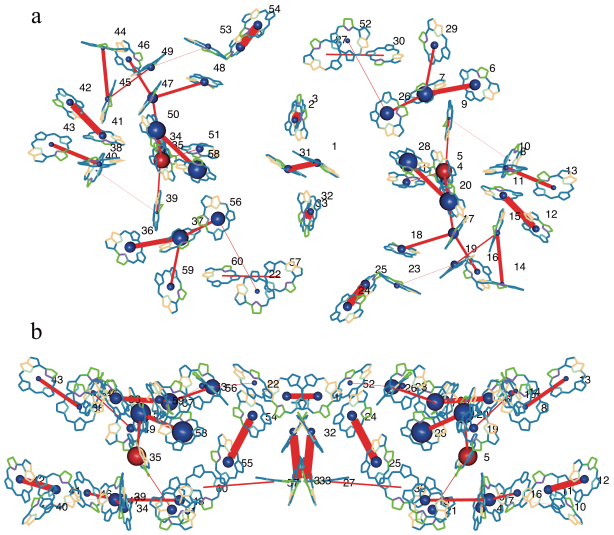

Figure 1: Arrangement of BChl-g, BCh-g', and Chl-a$_F$ and the distribution of excited state on hRC of *H. modesticaldum* (a: top view b: side view). Sizes of spheres at the centers of pigments indicate the distribution probabilities of the excited state in the lowest exciton state (No. 1 in Table 1), as calculated with the exciton model described in text. Red lines represent the networks of the highest excitation energy transfer probability between the pigments. Pigment arrangements were drawn using the R package 'Rpdb'[13] according to PDB data 5V8K.

sulfur bacteria (gRC) and heliobacteria (hRC) have long been unknown. These RCs belong to Type-I RCs showing low but clear homologies to PSI as for amino acid sequences of RC proteins and electron transfer cofactors. However, the structure with a high resolution at 2.2 Å was reported for the hRC of *Heliobacterium modesticaldum* recently.[12] The hRC consists of a homodimer of identical polypeptides having two-fold rotational symmetry and contains 54 bacteriochlorophyll (BChl) g, 4 BChl-g', and 2 8^1-hydroxychlorophyll a (Chl-a_F), as shown in Fig. 1 together with other cofactors, such as carotenoid (4,4'-diaponeurosporene) and iron sulfur center. The numbers on each pigment in the figure is in line with the one listed in the PDB file (5V8K).[12]

Determination of the hRC structure has allowed for the comparison of structures and functions of different Type I RCs in detail.[14] It will also potentially allow for greater understanding of the excitation transfer dynamics between BChl-g molecules on hRC. Pioneering studies on the isolated membranes of Heliobacteria[15–20] have shown the very fast and unique

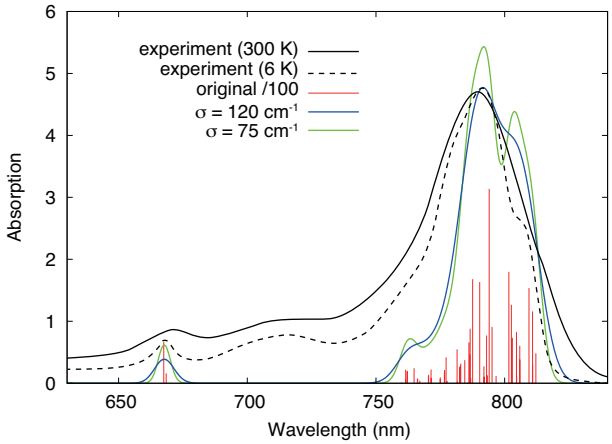

Figure 2: Reproduction of absorption spectrum of hRC. Each red bar indicates the absorption strength of individual exciton state listed in Table 1. The exciton strengths were weighted by Gaussian distribution with HWHM σ of 120 and 75 cm^{-1}, respectively, in Eq. (3) to simulate the spectra at room temperature and 6 K (blue and green curves), respectively. Experimentally obtained absorption spectra of hRC measured at room temperature and 6 K, which were reproduced after Refs. 21 and 16, are also shown as the black solid and broken lines, respectively. Note that the simulated spectra do not include the contributions of vibrational and Q_x bands that are present in experimental ones.

energy transfer dynamics suggesting the strong excitonic interaction, using ultrafast and selective excitation laser spectroscopy. However, functional studies on purified hRC of highly anaerobic heliobacteria are not many. The absorption spectrum of hRC in Fig. 2 consists of apparently three BChl-g component bands, which peak at 778, 793, and 808 nm in the cryogenic temperature measurement, and an absorption band of BChl-g' dimer that is an electron donor P800. Transient absorption spectroscopy at room temperature[16,17] has indicated that the 812 nm excitation laser induced the rapid uphill excitation transfer to the shorter-wavelength bands with a time constant (t_c) of 300 fs, and that the 770 nm excitation induced the downhill excitation transfer to the longer-wavelength bands with t_cs of 100 and 500 fs. On the other hand, the selective excitation of Chl-a (A_0) band at 670 nm induced a similar fast energy transfer process with more significant excitation/charge separation at P800.[16] We here theoretically analyzed the features of excitation transfer on hRC and compared with those on PSI or other RCs.

A comparison between the structures of hRC, PSI, and other RCs has been discussed

in detail recently.[14] The hRC contains multiple pigments in the locations almost homologous to those in PSI, which has 95 Chl-a in contrast to the 54 BChl-g, 4 BChl-g' and 2 Chl-a_F on hRC. Although the high-resolution hRC structure is now available, functional studies on purified hRC are not many yet. However, Heliobacteria have the light harvesting pigments only on hRC, with no extra antenna pigment complexes, so that the excitation energy absorbed by the pigments should be efficiently transferred to P800 inside hRC. It is noted that the spectroscopy performed on the membrane preparations[15–21] directly give the information for the process in hRC. The hRC structure also contain the components for electron transfer, which starts with the charge separation between P800 and A_0, to give an electron to iron sulfur center F_X, as in PSI. The existence/function of the electron acceptor A_1, which is phylloquinone that mediates electron transfer between A_0 and F_X in PSI and probably menaquinone in hRC, is still puzzling in hRC.[9,12] Majorities of PSI RCs are known to contain a few molecules of special Chl-a forms known as "red-Chl-a", which give the longer-wavelength absorption/fluorescence bands adjacent to the PSI major bands and accept excitation energy from major bands with a time constant of around 10 ps at 77 K[1,8]. On the other hand, hRCs appears to contain no red-Chl-g bands as seen from the absorption spectrum in Fig. 2 or from the 77 K-fluorescence spectrum with the red-most peak at around 810 nm.[22]

Theoretical analysis of the excitation transfer dynamics on hRC is scarce. Formulation of a reliable theoretical model requires the location and site energy of each pigment, excitonic interactions between the pigments, interaction between their excited state molecular orbitals of their excited state, and the nuclear vibrational states of surrounding environments. We here formulated a simple model that is useful for the analysis of excited state dynamics and to know the features of hRC by applying the Frenkel exciton theory.[23] We adopted reliable parameters for the chemical natures of pigments from previously reported values and used the location/geometry of each pigment on the hRC structure. We, however, set the site energy to be constant for most of the BChl-g molecules to make the situation simpler and to highlight

the role of pigment arrangement on the hRC structure. The exciton state model formulated for the geometries of 54 BChl-g, 4 BChl-g' and 2 Chl-a on hRC qualitatively reproduced the absorption spectrum of the hRC as shown in Fig. 2. The model also enabled numerical analysis of the exciton dynamics, which can be compared with the decay associated spectra obtained by laser spectroscopy experiments.[17] The model describes the delocalized exciton states of BChl-g on hRC with coherency stronger than that of Chl-a on the PSI reaction center. It seems to be mainly due to the stronger transition-dipole moment on BChl-g on hRC, in addition to the effect of assumption of equal site energies that increase the coherency. The high-resolution hRC structure, thus, gave us an opportunity to propose a simple exciton model useful for the theoretical/experimental analysis of excited state dynamics on hRC.

In the following, we describe the new model, numerical results using the new model, and discuss the numerically obtained results on absorption spectrum and energy transfer process. Theoretical methods are described in the Appendices.

Numerical results

Theoretical model

We calculate the excitonic interaction V_{ij} between i-th and j-th pigments as transition-dipole interaction of Eq. (1). We adopt the position $\boldsymbol{r}_i$ of the transition-dipole moment of the i-th pigment to position of Mg in PDB data list of hRC.[12] We used the following parameters: the relative dielectric constant is 1, the strength of transition-dipole moment $|\boldsymbol{\mu}_i|$ is 6.5 debye,[24,25] and the direction of transition-dipole moment $\boldsymbol{\mu}_i/|\boldsymbol{\mu}_i|$ is defined from the distance vector between the positions of NB and ND of BChls and Chl-a_F in PDB data.

It should be noticed that we defined the excitonic interaction value between BChl-g of P800 as 250 cm^{-1}. We estimated this value from the comparison with P700. The structure of P800 resembles that of P700 so that we multiplied the value of 138 cm^{-1} of excitonic interaction between Chl-a and Chl-a' of P700 by a factor of $(6.5/4.8)^2$ and obtained a value

of 250 cm^{-1} of excitonic interaction for P800 because the transition dipole moment of BChl-g and Chl-a are 6.5 and 4.8 debye, respectively. The value of 250 cm^{-1}, thus, assumed, also meets the one estimated for the interaction between the nearest BChl-a molecules (B850) in LH2,[26] which shows the strong excitonic interaction. On the other hand, the direct numerical calculation of the excitonic interaction between BChl-g molecules of P800 gave the extraordinary high value of 1025 cm^{-1}, probably due to the overestimation that comes simply from the short 6 Å distance between the two central Mg atoms of P800 in the hRC structure.[12]

All site energies E_i for the BChl-g and BChl-g' are equally set at 785 nm, except for the site energy for the Chl-a_F that is set at 670 nm. We used the HWHM σ as 120 or 75 cm^{-1} for the Gaussian line shapes to give the inhomogeneous distribution to dress the stick (one value) presentation of exciton spectra at room temperature or 6 K shown in Fig. 2.

Exciton states

Table 1 lists the numerical values of E_ν for all exciton states ν obtained by solving the eigenvalue problem. We firstly estimated the number of pigments, which are delocalized in an exciton eigenstate, by analyzing the inverse of participation ratios N_ν of Eq. (2). Altogether 60 eigenstates from the lowest (No.1 at 812 nm) to the highest (No. 60 at 667.6 nm) energy levels were determined on pigments on the hRC as listed in Table 1.

The spheres on central Mg atom in Figure 1 represent the distribution probability of excitation energy on each pigment in the lowest exciton state (No. 1 at 812 nm) in Table 1. All the exciton states listed in Table 1 are delocalized over at least 4-6 pigments and at the maximum 27 pigments, as can be seen in Fig. 3. The transition-dipole moment of BChl is 1.5 times larger than that of Chl-a and therefore, the magnitude of the excitonic interaction between BChl-g molecules on hRC becomes larger than that between Chl-a molecules in PSI, although the number of BChl-g and consequently the density of pigments on hRC, is almost half of that of Chl-a on PSI.

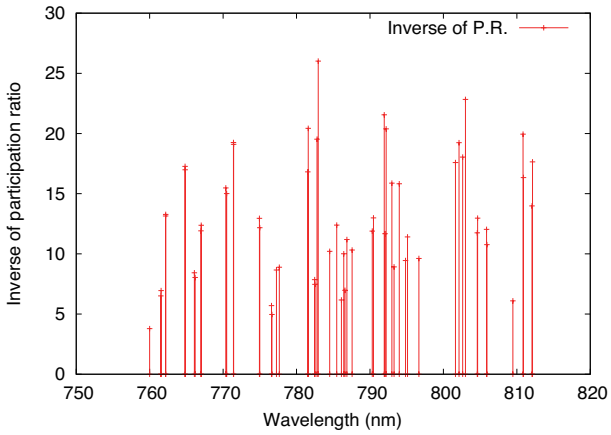

Figure 3: Relation between the eigen-energies of exciton states E_ν and inverse of participation ratio N_ν of Eq. (2), calculated by the new exciton model numerically. E_ν is expressed in wavelength unit. It is noted that two N_ν values exist in some excitonic states in the degenerate state and contribute to E_ν. See text in details.

To analyze the exciton dynamics among the randomly arranged pigments a method of dividing into certain domains can be adopted.[3] The pigments are determined to be in the same domain when the excitonic interaction V_{ij} of i-th and j-th pigment are larger than the reorganization energy λ of each pigment. Then, theoretical analysis within the domain is performed by delocalized exciton dynamics by Redfield theory.[27] In contrast, analysis of energy transfer between the different domains can be performed by generalized Förster theory.[28,29] From the analysis of inverse of participation ratio in Fig. 3 and of the method of dividing into certain domains, it was shown that the spatial extent of the exciton state extends to the entire hRC system owing to the small value of $\lambda = 36$ cm^{-1}.[3] Hence, in the following numerical analysis, we applied only Redfield theory to the numerical analysis of exciton dynamics.

Reproduction of absorption spectrum

By using Eq. (3), we numerically calculated the absorption spectrum of hRC using the result in Table 1 and the selected bandwidth (HWHM) σ. The spectrum obtained with $\sigma = 75$ cm^{-1}[2] in Fig. 2 represents the predicted absorption spectrum at cryogenic temperature 6

Table 1: Numerically obtained eigen-energies E_ν (expressed in nm) for a number of each exciton state ν.

ν	E_ν	ν	E_ν	ν	E_ν	ν	E_ν
1	812.1	16	794.8	31	784.5	46	770.5
2	812.1	17	794.0	32	782.9	47	770.4
3	810.9	18	793.3	33	782.8	48	767.0
4	810.8	19	793.0	34	782.5	49	767.0
5	809.5	20	792.2	35	782.5	50	766.2
6	805.9	21	792.0	36	781.6	51	766.1
7	805.9	22	791.9	37	781.5	52	764.8
8	804.7	23	790.5	38	777.7	53	764.8
9	804.6	24	790.3	39	777.3	54	762.2
10	803.0	25	787.6	40	776.6	55	762.2
11	802.6	26	786.9	41	776.6	56	761.6
12	802.1	27	786.6	42	775.0	57	761.5
13	801.6	28	786.4	43	775.0	58	760.0
14	796.7	29	786.1	44	771.4	59	668.5
15	795.1	30	785.5	45	771.4	60	667.6

K.[16] The three peak positions around 800 nm obtained by numerical calculation were similar to those of the experimentally obtained absorption spectrum, which mainly consists of three bands. We also showed the numerical result with $\sigma = 120$ cm^{-1} to reproduce the experiment at room temperature[17] although the σ value is a little larger than that used in Ref. 2. It is noted that the calculated spectra in Fig. 2 only show the Q_y transition bands and do not contain contributions of the vibrational or Q_x bands etc, which contribute to the actual absorption spectra in the shorter wavelength side.

Predicted distributions of excited states calculated by the model

In the ν-th exciton state, the probability that the i-th pigment is in excited state equals to $|C_\nu^i|^2$. Fig. 1 shows the probability of excitation of pigments in delocalized lowest exciton state ($\nu = 1$ at 811.2 nm) in hRC obtained based on the numerical calculation of exciton states. The excitation probabilities of pigments are shown by the sphere sizes at the Mg positions of BChl-g molecules. The volume of the sphere is set to be proportional to the excitation probability. It was observed that the excited state resides on multiple BChl-g

molecules in this lowest energy exciton state. In the other lower energy states at ν = 2-4 that gave energy values at 812.1 to 810.8 nm, excitation energy was distributed to these or nearby BChl-g molecules (see Fig. S1 in SI) In contrast, excitation energy resides on special pair P800 in the 5th (809.5 nm) and 14th (796.7 nm) exciton states as listed in Table 1. Therefore, these two states have larger excitation probabilities on P800 and seem to be important for the energy accumulation from antenna BChl-g to P800.

The pairs of pigments connected by solid red lines in Fig. 1 gave the largest squared value, V_{ij}^2, of the excitonic coupling from the i-th to j-th pigment. It is seen from Fig. 1 that the pigments in hRC are aligned nearly in two layers at different depths from the membrane surface. BChl-g'-5 (or BChl-g'-35) is connected to BChl-g-20 (or BChl-g-50) and BChl-g-28 (BChl-g-58) in this exciton state. Therefore, these pigments have larger probabilities of excitation in this state. If we focus on the localized excitation energy transfer, the networks in Fig. 1 correspond to the fastest energy transfer path between the two pigments with Förster rate formula Eq. (4).

Energy transfer dynamics: Calculation of decay associated spectra based on the model

Figure 4 shows the analysis of energy transfer through the calculation of decay associated spectra (DAS)[30] obtained by using Eq. (10). Energy transfer processes between the exciton states were calculated according to the model after imaginal excitation of the system with either 770 nm laser pulse with a 30 fs HWHM or 812 nm laser pulse with a 60 fs HWHM to reproduce the experiments of the transient absorption spectroscopy performed at room temperature.[17] The vertical axis in Fig. 4 represents the number of α-th eigenstate with the lifetime $1/R_\alpha$ of Eq. (8), i.e., longer time at the larger α as seen from right hand scale and Fig. 5. In Fig. 4, the blue and red regions in the DAS show the decay and increase in population in each exciton state, respectively. Hence energy transfer occurs with the time constant $1/R_\alpha$ from the blue to the red wavelength region for a given α value. After 770

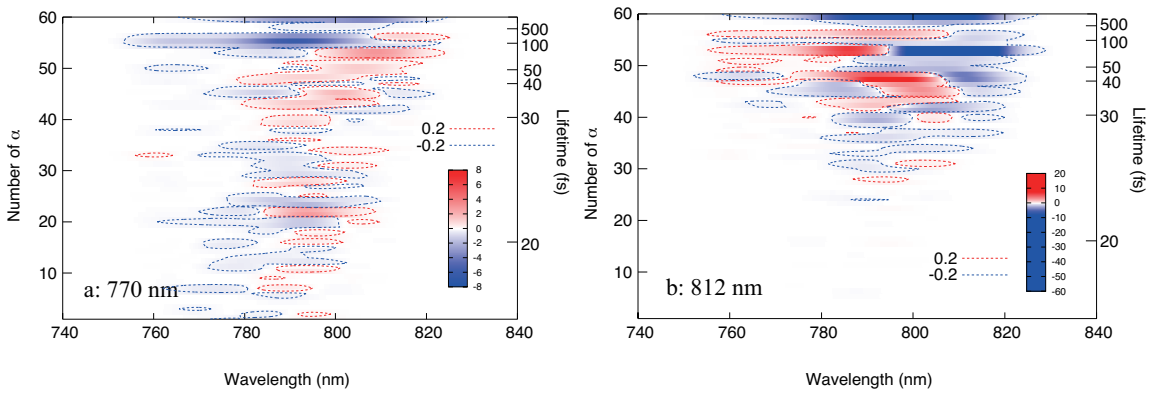

Figure 4: DAS-type analysis obtained by the numerical calculation of exciton states after selective excitations of hRC. Vertical axis represents α value. At the larger α, the shorter lifetime of the exciton state (see Fig. 5). See text for details. a) After excitation at 770 nm with 30 fs HWHM. b) After excitation at 812 nm with 60 fs HWHM. Blue and red lines indicate decrease and increase, respectively, of excitation at the indicated wavelength ranges. The lower population regions above/below 0.2 relative unit are surrounded by broken lines.

nm photo-excitation, transition of the excited state occurs from 760 nm to 820 nm. There are many negative distributions that indicate depression at α from 1 to 50. In contrast, excitation at 812 nm induces negative distributions in the DAS, mostly in the region from 780 to 820 nm at α 30-50. These results reproduce the DAS experimentally obtained by laser spectroscopy, which measured the absorption changes in the membranes after selective excitations by the 770 or 812 nm laser.[17] Therefore, the analysis based on the present model is shown to be useful for the interpretation/understanding of excitation dynamics on hRC.

Figure 5 shows the lifetime $1/R_\alpha$ of α-th eigenstate in DAS analysis. At α from 1 to 55,

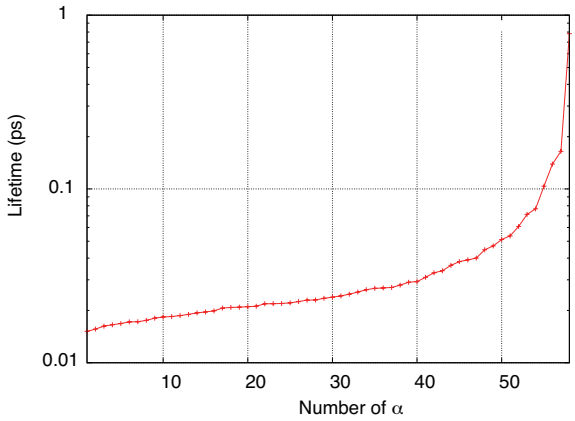

Figure 5: Dependencies of lifetime $1/R_\alpha$ on α value

the lifetime is less than 100 fs. At α over 55, the lifetime drastically increased to to 1 ps or longer because the energy trapping for charge separation is not included in the present model.

Discussion

Theoretical DAS analysis in Fig. 4 suggested complicated relaxation dynamics in the high energy region over 800 nm in the time scale of the lifetime less than 100 fs after excitation at 770 nm. The excited energy is relaxed into the excited states at 790 nm and 810 nm at 100 fs to 1 ps.

We calculated spectral changes as the decay associated spectrum (DAS) at different time ranges from Figs. 4 and 5. Fig. 6a shows the DAS at α = 53-58 when the excitation wavelength is 770 nm. The lifetimes of the states with α at 53 and 56 are $1/R_{53}$ =71 fs, and $1/R_{56}$ = 139 fs, respectively as seen from Fig. 5. The DAS of $\alpha = 53$ gave a negative peak at around 790 nm and a positive peak at around 810 nm, indicating that the downhill EET takes place from 790 nm to 810 nm in the timescale of 70 fs and 140 fs. In contrast, Fig. 6b shows the DAS of α = 53-58 for excitation at 812 nm. The DAS of $\alpha = 53$ has a negative peak at around 810 nm and a positive peak at around 790 nm, indicating that the uphill EET takes place from 810 nm to 790 nm in the timescale of 70 fs. The shapes of DAS are qualitatively the same in the case of $\alpha = 53$ for 770 and 812 nm photo-excitations. We can detect the peaks at 790, 800 and 810 nm in Fig. 6 in agreement with the experimentally observed peaks at 778, 793, and 808 nm.[17]

Fig. 7 shows the EET scheme obtained by numerical analysis. It is almost comparable to the experimental observation.[17] The EET timescales predicted by our analysis is, therefore, similar to those detected by the experiment although the time scales are a little shorter in the former. This indicates that the simple exciton model can be applied to interpret the exciton dynamics on hRC, at least qualitatively.

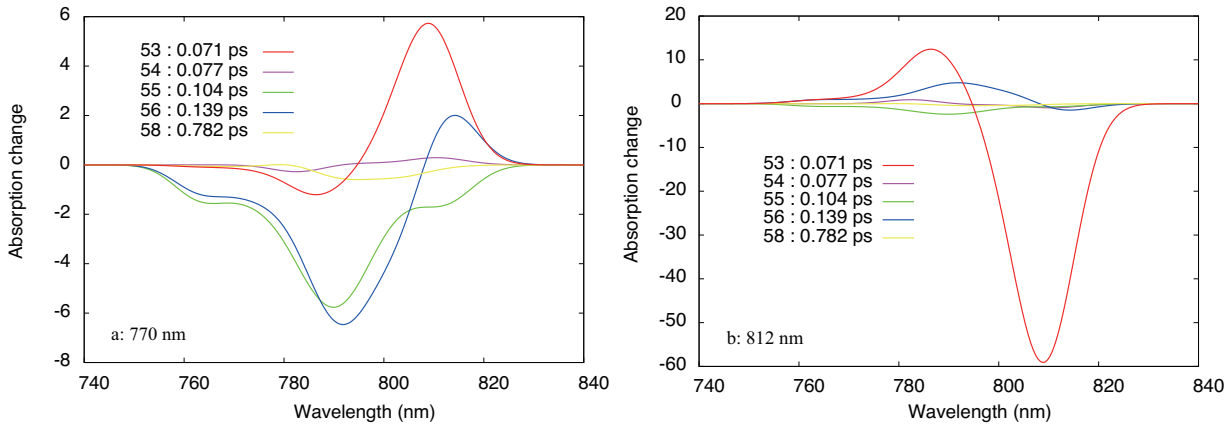

Figure 6: DAS of $\alpha = 53$, 54, 55, 56 and 58. a) excited at 770 nm pulse. b) excited at 812 nm pulse.

Experiments have also revealed that EET to P800 occurs rapidly within 0.5 ps when Chl-a is excited.[16] When Chl-a is excited by a pulse laser of 670 nm, the excited state is sometimes localized on Chl-a. In the process of relaxation to the lower excited state, the excitation energy must be transferred to other antenna pigments. Although the EET rate can be estimated by the generalized Förster theory,[29] the overlap-integral between the emission spectrum of Chl-a and the density of exciton states of BChl-g in hRC is too small in the present model. Hence, the reaction rate is quantitatively estimated to be too slow. However, considering the nuclear vibrational states for the 0-1 transition process in the light absorption of each pigment, the value of overlap-integral of the exciton state can be increased.[31] In addition, if the excitonic interaction between Chl-a and its nearest BChl-g gives a large value, the short relaxation time constant detected by the experiment will be reproduced.

The exciton state in hRC tends to be coherent in hRC. It is mainly due to the stronger excitonic interaction between BChl-g, which has a transition-dipole moment stronger than that on Chl-a. Therefore, the excitation energy on antenna BChl-g on hRC is likely to be more delocalized than that on Chl-a on PSI and PSII. In PSI, the reproduction of absorption spectrum is reported to be rather difficult if only the homogeneous site energy is applied.[2] Thus, additional fine adjustment of site energy for each Chl-a was necessary to reproduce the

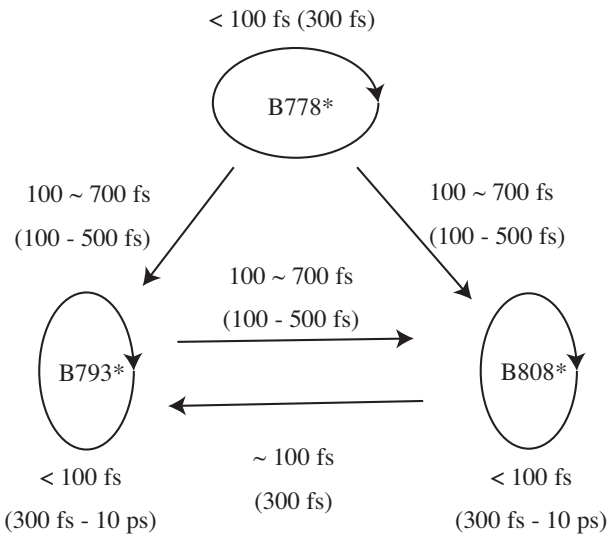

Figure 7: Schemes of exciton relaxation in hRC at room temperature. Values estimated in this study are given to the scheme and time constants (in parenthesis) originally proposed by the experimental measurement of hRC in Ref. 17.

rational absorption spectrum of PSI. Similar situations are reported for PSII.[3,4] In contrast, the absorption spectrum of hRC was reproduced rather well even when the site energies were set at the same value for all BChl-g and BChl-g' molecules in our model. Therefore, this type of simple model is also useful for analyzing energy transfer dynamics on hRC. The values of lifetimes $1/R_\nu$ given by our model are rather faster than those detected by the experiment. This is assumed to be caused by the simple model that artificially assumed the equal site energies of BChls because this assumption should have increased the electronic coherency in the system. The addition of static disorder into site energies will weaken the electronic coherency and will make the energy transfer rate slower. In the numerical analysis by the Redfield formula, we used the spectral density $J(\omega)$ of Eq. (6), which results in a reorganization energy of about 100 cm^{-1}.[32] A three times smaller reorganization energy was reported for the core complex of PSII.[3] Assuming that the reorganization energy of the present system is similar, it would result in three times smaller Redfield rate constants of exciton relaxation. In order to determine the reorganization energy for the present system, an analysis of the temperature-dependence of absorption spectra could be used.[3] In the calculations of excitonic couplings we took into account the transition dipole moment of

BChl-g in vacuum and neglected any screening/local field correction effects of the excitonic couplings by the polarization of the medium. The latter effects have been estimated to result in an effective screening factor of 0.7 for the couplings in PSI.[33] Taking into account this factor, that is, a reduction of the excitonic couplings by 30 percent, in the limit of weak couplings, would result in a reduction of the rate constant by a factor of 2. Hence, the rescaling of the spectral density by a factor of three and the reduction of the excitonic couplings by 30 percent would result in relaxation rates smaller by roughly a factor of six. In the future, modification of site energies as well as the fine adjustment of inhomogeneous broadenings will provide a better reproduction of hRC absorption spectrum as reported for PSI[2] as well as of the EET rate to reproduce the experimental values.

According to the DAS-type representation of exciton relaxation by Redfield theory shown in Fig. 4, we found that the lifetime extends from 10 fs to 1 ps and almost reproduces the experimental observation in hRC. DAS became all blue (depletion of ground state) at α close to 60 in Fig. 4. These states, therefore, show no more energy transfer to the other exciton state after accumulating the excitation energy. They are, on the other hand, expected to transfer energy to the charge separation reaction although it is not included in the present model. It is interesting that P800 and BChl-g monomers adjacent to P800 (so-called accessory BChls) show the largest contribution in the 5th and 14th lowest energy states. The charge separation between P800 and A_0 occurs with a 10 ps lifetime in parallel with the excitation transfer in hRC.[17] Hence, the spectral changes in the long-time region will be better reproduced if the contribution of electron transfer reaction is incorporated into the present exciton model. It will be interesting to predict the temperature dependence of primary charge separation resulting from the contributions of the primary electron donor to the different exciton states in the future.

In the numerical studies in PSI,[5–8] it has been reported that one specific Chl-a near the center of PSI functions as the hub for the energy transfer network. It is not yet clear whether some BChl-g molecules in hRC might serve the same hub function. The present exciton state

model will be also useful to test the role of each BChl-g molecule. The timescale of energy transfer from antenna Chl-a to the special pair in PSII, which is around 40-50 ps,[3,4] is much longer than the corresponding timescale in hRC. The results of the present study suggest that the weaker coherence of the exciton states formed between the antenna Chl-a molecules as well as the weaker transition-dipole moment on each Chl-a may explain the slower excitation energy transfer rates in PSII or PSI. The evolutional relationships between the mechanisms of exciton dynamics in different RCs will be better understood with our new model for hRC.

The simple model proposed in this study will be useful in the study of RC functions. Fig. 1 shows the distribution of excitation energy and the networks involved in the excitation transfer between the pigments in the lowest exciton state in Table 1. The probability of excitation is shown as the sphere volume on each pigment. The figure for this exciton state indicates that BChl-g'-5 and BChl-g'-35 mediate the excitation transfer between the other pigments in the two separated layers beneath each surface of the membrane. Artificial removal of BChl-g' by the genetic modification of the amino acid residues coordinated to their central Mg atoms, therefore, is expected to modify the lowest exciton state to be replaced by the other exciton state. The simple exciton model, thus, predicts a significant change in the total exciton dynamics on hRC by the point mutation. Similar experiments may be useful for studying the structure unknown green sulfur RC (gRC), which is known to have an analogous structure with BChl-a. BChl-a has a strong dipole moment as BChl-g so that the exciton model as used for hRC seems to be useful too. The number of pigments on gRC is lower than that on hRC[34,35] so that the absorption spectrum of gRC is simpler and is expected to be suited for the analysis of exciton dynamics.

Antenna systems of both type-I and type-II bacteria using BChl-a, such as LHI, LHII, and FMO, seem to benefit by the use of strongly exciton-coupled BChl-a molecules that have strong dipoles. In contrast, the PSII antenna is composed of rather weakly exciton-coupled Chl-a, (or Chl-d in *Acaryouchloris* that has Chl-d based PSI and PSII[36]). The extent of delocalized excitation energy generated on excitonic coupling on PSI is also assumed to

be weaker than that generated by hRC. The present exciton state model, thus, provides a foundation for further in silico experiments to explore the functionality. The energy transfer dynamics of hRC artificially modified to harbor BChl-a or Chl-a instead of BChl-g is also interesting because such virtual experiments are necessary to pursue the evolution of RCs.

Conclusion

We propose here a simple theoretical model of exciton dynamics based on the high-resolution structure of hRC and successfully reproduced the absorption spectrum of hRC. The site energies for BChl-g and BChl-g' in the new model have not been determined, and single values were adopted for all, except for Chl-a_F. This simple model allowed calculation of the excitonic interaction based on the transition-dipole interaction. The exciton states calculated by the model suggested stronger electronic coherences due to the excitonic interaction being stronger than that in PSI and PSII owing to the use of different chlorophyll species. The rates between each exciton state were calculated using the Redfield theory by considering the exciton-phonon coupling in the framework of reported model.[32] Based on the calculated relaxation rates, we analyzed the time scale of the exciton dynamics by DAS analysis to interpret the experimental results. This new model will help understanding the evolution/origin of the mechanisms of light harvesting processes in RCs.

Appendix

The total electronic Hamiltonian H is defined as follows. The diagonal element of the Hamiltonian H_{ii} is the site energy E_i in the site representation, and the off-diagonal element H_{ij} is the excitonic interaction V_{ij} between site i and j. Using the Hamiltonian, we numerically solved the eigenvalue problem as the Schrödinger equation $H\Psi_\nu = E_\nu\Psi_\nu$ where E_ν is the eigenvalue of the ν-th exciton state, and its exciton state Ψ_ν is expressed as the following eigenvector: $\Psi_\nu = (C_\nu^1, C_\nu^2, \cdots, C_\nu^i, \cdots, C_\nu^{(N-1)}, C_\nu^N)^t$ where C_ν^i is the probabilistic amplitude

at the i-th site in the ν-th exciton state.

The transition-dipole interaction V_{ij} is expressed as follows:

$$V_{ij} = \frac{1}{4\pi\epsilon}\left[\frac{(\boldsymbol{\mu}_i \cdot \boldsymbol{\mu}_j)}{\boldsymbol{r}_{ij}^3} - \frac{3(\boldsymbol{\mu}_i \cdot \boldsymbol{r}_i)(\boldsymbol{\mu}_j \cdot \boldsymbol{r}_j)}{\boldsymbol{r}_{ij}^5}\right], \tag{1}$$

where $\boldsymbol{\mu}_i$ is the vector of the transition-dipole moment of the i-th pigment, $\boldsymbol{r}_i$ is its position vector, and $\boldsymbol{r}_{ij}$ is the distance vector defined as $\boldsymbol{r}_i - \boldsymbol{r}_j$.

The inverse of the participation ratio N_ν can be used to estimate the pigment number of delocalization in the exciton state ν. This can be defined as follows:

$$N_\nu = \frac{1}{\sum_i |C_\nu^i|^4}. \tag{2}$$

These calculations of the exciton states yield the transition-dipole moment $\boldsymbol{\mu}_\nu$ for each exciton state ν. It is expressed as the linear combination of the transition-dipole moments $\boldsymbol{\mu}_i$ by the site representation as $\boldsymbol{\mu}_\nu = \sum_{i=1}^N C_\nu^i \boldsymbol{\mu}_i$. Since the oscillator strength for each exciton state ν is proportional to $|\boldsymbol{\mu}_\nu|^2$, the Gaussian distribution with the HWHM σ to reproduce the absorption spectrum in the experiment is introduced as follows:

$$A(E) = A_0 \sum_{\nu=1}^{N} |\boldsymbol{\mu}_\nu|^2 \exp[-(E - E_\nu)^2/\sigma^2], \tag{3}$$

where A_0 is the normalization factor.

The Förster's rate formula[28] is expressed as

$$k_{ij}^F = \frac{2\pi V_{ij}^2}{\hbar} \int dE A_i(E) E_j(E), \tag{4}$$

where $E_j(E)$ is the emission spectrum of the j-th molecule, and $A_i(E)$ is the absorption spectrum of the j-th molecule. In this study, because the site energies of each molecule are the same, except for the Chl-a, the overlap integral in the rate formula is constant when

i and j are BChl-g or BChl-g'. Hence, the numerical analysis was conducted only for the normalized rate defined as $k_{ij}^F = CV_{ij}^2$, where C is constant.

The Redfield formula[27] is expressed as

$$k_{\mu\nu}^R = 2\pi \sum_{i=1}^{N} \Omega_{\nu\mu}^2 (C_i^\mu C_i^\nu)^2 J(\Omega_{\nu\mu})(n(\Omega_{\nu\mu}) + 1), \tag{5}$$

where $J(\Omega_{\nu\mu})$ is the density of the states of phonon, $n(\Omega_{\nu\mu})$ is the Bose-Einstein distribution function, and $\Omega_{\nu\mu}$ is defined as the $(E_\nu - E_\mu)/\hbar$. In particular, we use the function $J(\omega)$ as follows:

$$J(\omega) = \sum_{n=1,2} \frac{s_n}{7!2\omega_n^4} \omega^3 e^{-(\omega/\omega_n)^{1/2}}, \tag{6}$$

where each parameter is defined as $s_1 = 0.8$, $s_2 = 0.5$, $\hbar\omega_1 = 0.069$ meV, and $\hbar\omega_2 = 0.24$ meV, respectively.[32]

The time dependency of the emission strength is proportional to the following expression:

$$\sum_\nu |\boldsymbol{\mu}_\nu|^2 \rho_\nu(t) = \sum_{\alpha,\nu,\mu} |\boldsymbol{\mu}_\nu|^2 U_{\nu\alpha} U_{\alpha\mu}^{-1} e^{-R_\alpha t} \rho_\mu(0), \tag{7}$$

where we defined the probability of the ν-th exciton state that satisfies the master equation based on the Redfield equation as $\dot{\rho}_\mu(t) = -\sum_\nu k_{\mu\nu}^R \rho_\nu(t)$. The matrix $k_{\mu\nu}^R$ of Eq. (5) was diagonalized by the diagonalization matrix $U_{\nu\alpha}$ for the eigenvalue R_α defined as

$$R_\alpha = \sum_{\mu\nu} U_{\alpha\mu}^{-1} k_{\mu\nu}^R U_{\nu\alpha}. \tag{8}$$

According to the definition of the DAS analysis,[30] the formula is expressed as

$$\mathrm{DAS}_\alpha = \sum_{\mu,\nu} |\boldsymbol{\mu}_\mu|^2 U_{\mu\alpha} U_{\alpha\nu}^{-1} \rho_\nu(0). \tag{9}$$

To compare the experimentally obtained DAS with those obtained theoretically, we introduce the Gaussian distribution with the HWHM σ to DAS as follows:

$$\mathrm{DAS}_\alpha(E) = \sum_{\mu,\nu} |\boldsymbol{\mu}_\mu|^2 U_{\mu\alpha} U^{-1}_{\alpha\nu} \rho_\nu(0) e^{-(E-E_\mu)^2/\sigma^2}. \tag{10}$$

We defined the initial condition $\rho_\nu(0)$ as

$$\rho_\nu(0) = \frac{|\boldsymbol{\mu}_\nu|^2 e^{-(E_0-E_\nu)^2/\sigma_0^2}}{\sum_\mu |\boldsymbol{\mu}_\mu|^2 e^{-(E_0-E_\mu)^2/\sigma_0^2}}, \tag{11}$$

where E_0 is the energy of the incident photon, and σ_0 is the HWHM of the spectrum of the incident photon.

Acknowledgments

This work was supported by a grant from KAKENHI (Grant Numbers 17K07440) to S.I. The authors are grateful to Drs. Hirozo Oh-oka of Osaka University, Chihiro Azai of Ritsumeikan University and Toru Kondo of Massachusetts Institute of Technology and for their valuable discussions during the study.

Supporting Information Available

Dataset of the excitonic couplings used in the calculation. Graphical arrangements of the distribution probabilities of the excited state at BChl-g, BCh-g', and Chl-a$_F$ on hRC for each exciton state from No. 1 to 60.

References

(1) Heathcote, P.; Jones, M. R.; Fyfe, P. K. Type I photosynthetic reaction centres: structure and function. *Phil. Trans. R. Soc. Lond. B* **2003**, *358*, 231–243.

(2) Vaitekonis, S.; Trinkunas, G.; Valkunas, L. Red Chlorophylls in the Exciton Model of Photosystem I. *Photosynth. Res.* **2005**, *86*, 185–201.

(3) Raszewski, G.; Renger, T. Light Harvesting in Photosystem II Core Complexes Is Limited by the Transfer to the Trap: Can the Core Complex Turn into a Photoprotective Mode? *J. Am. Chem. Soc.* **2008**, *130*, 4431–4446.

(4) Shibata, Y.; Nishi, S.; Kawakami, K.; Shen, J.-R.; Renger, T. Photosystem II Does Not Possess a Simple Excitation Energy Funnel: Time-Resolved Fluorescence Spectroscopy Meets Theory. *J. Am. Chem. Soc.* **2013**, *135*, 6903–6914.

(5) Sener, M. K.; Lu, D.; Ritz, T.; Park, S.; Fromme, P.; Schulten, K. Robustness and Optimality of Light Harvesting in Cyanobacterial Photosystem I. *J. Phys. Chem. B* **2002**, *106*, 7948–7960.

(6) Yang, M.; Damjanović, A.; Vaswani, H. M.; Fleming, G. R. Energy Transfer in Photosystem I of Cyanobacteria *Synechococcus elongatus*: Model Study with Structure-Based Semi-Empirical Hamiltonian and Experimental Spectral Density. *Biophys. J.* **2003**, *85*, 140 – 158.

(7) Abramavicius, D.; Mukamel, S. Exciton Delocalization and Transport in Photosystem I of Cyanobacteria *Synechococcus elongates*: Simulation Study of Coherent Two-Dimensional Optical Signals. *J. Phys. Chem. B* **2009**, *113*, 6097–6108.

(8) Shibata, Y.; Yamagishi, A.; Kawamoto, S.; Noji, T.; Itoh, S. Kinetically Distinct Three Red Chlorophylls in Photosystem I of *Thermosynechococcus elongatus* Revealed by Femtosecond Time-Resolved Fluorescence Spectroscopy at 15 K. *J. Phys. Chem. B* **2010**, *114*, 2954–2963.

(9) Kondo, T.; Matsuoka, M.; Azai, C.; Kobayashi, M.; Itoh, S.; Oh-oka, H. Light-Induced Electron Spin-Polarized (ESP) EPR Signal of the $P800^+$ Menaquinone$^-$ Radical Pair

State in Oriented Membranes of *Heliobacterium modesticaldum*: Role/Location of Menaquinone in the Homodimeric Type I Reaction Center. *J. Phys. Chem. B* **2018**, *122*, 2536–2543.

(10) Jordan, P.; Fromme, P.; Witt, H. T.; Klukas, O.; Saenger, W.; Krauß, N. Three-dimensional structure of cyanobacterial photosystem I at 2.5 Å resolution. *Nature* **2001**, *411*, 909–917.

(11) Umena, Y.; Kawakami, K.; Shen, J.-R.; Kamiya, N. Crystal structure of oxygen-evolving photosystem II at a resolution of 1.9 Å. *Nature* **2011**, *473*, 55–61.

(12) Gisriel, C.; Sarrou, I.; Ferlez, B.; Golbeck, J. H.; Redding, K. E.; Fromme, R. Structure of a symmetric photosynthetic reaction center–photosystem. *Science* **2017**, *357*, 1021–1025.

(13) Idé, J. Read, Write, Visualize and Manipulate PDB Files. 2017; R package version 1.14.4 — For new features, see the 'Changelog' file (in the package source).

(14) Orf, G. S.; Gisriel, C.; Redding, K. E. Evolution of photosynthetic reaction centers: insights from the structure of the heliobacterial reaction center. *Photosynth. Res.* **2018**, 1–27.

(15) Trost, J. T.; Blankenship, R. E. Isolation of a photoactive photosynthetic reaction center-core antenna complex from *Heliobacillus mobilis*. *Biochemistry* **1989**, *28*, 9898–9904.

(16) Neerken, S.; Aartsma, T. J.; Amesz, J. Pathways of Energy Transformation in Antenna Reaction Center Complexes of *Heliobacillus mobilis*. *Biochemistry* **2000**, *39*, 3297–3303.

(17) Liebl, U.; Lambry, J.-C.; Leibl, W.; Breton, J.; Martin, J.-L.; Vos, M. H. Energy and Electron Transfer upon Selective Femtosecond Excitation of Pigments in Membranes of *Heliobacillus mobilis*. *Biochemistry* **1996**, *35*, 9925–9934.

(18) Nuijs, A. M.; Dorssen, R. J. v.; Duysens, L. N. M.; Amesz, J. Excited states and primary photochemical reactions in the photosynthetic bacterium *Heliobacterium chlorum*. *PNAS* **1985**, *82*, 6865–6868.

(19) Noort, P. I. V.; Gormin, D. A.; Aartsma, T. J.; Amesz, J. Energy transfer and primary charge separation in *Heliobacterium chlorum* studied by picosecond time-resolved transient absorption spectroscopy. *BBA-Bioenergetics* **1992**, *1140*, 15 – 21.

(20) Lin, S.; Chiou, H.; Kleinherenbrink, F.; Blankenship, R. Time-resolved spectroscopy of energy and electron transfer processes in the photosynthetic bacterium *Heliobacillus mobilis*. *Biophys. J.* **1994**, *66*, 437 – 445.

(21) Miyamoto, R.; Iwaki, M.; Mino, H.; Harada, J.; Itoh, S.; Oh-oka, H. ESR Signal of the Iron − Sulfur Center FX and Its Function in the Homodimeric Reaction Center of *Heliobacterium modesticaldum*. *Biochemistry* **2006**, *45*, 6306–6316.

(22) Sarrou, I.; Khan, Z.; Cowgill, J.; Lin, S.; Brune, D.; Romberger, S.; Golbeck, J. H.; Redding, K. E. Purification of the photosynthetic reaction center from *Heliobacterium modesticaldum*. *Photosynth. Res.* **2012**, *111*, 291–302.

(23) Frenkel, J. On the Transformation of light into Heat in Solids. I. *Phys. Rev.* **1931**, *37*, 17–44.

(24) Knox, R. S.; Spring, B. Q. Dipole Strengths in the Chlorophylls. *Photochem. Photobiol.* **2003**, *77*, 497–501.

(25) Pessarakli, M. E. *Handbook of Photosynthesis, Third Edition. Boca Raton*; CRC Press., 2016.

(26) Cogdell, R. J.; Gall, A.; Köhler, J. The architecture and function of the light-harvesting apparatus of purple bacteria: from single molecules to in vivo membranes. *Q. Rev. Biophys.* **2006**, *39*, 227–324.

(27) Redfield, A. G. On the Theory of Relaxation Processes. *IBM J. Res. Dev.* **1957**, *1*, 19–31.

(28) Förster, T. Zwischenmolekulare Energiewanderung und Fluoreszenz. *Ann. Phys. (Leipzig)* **1948**, *437*, 55–75.

(29) Sumi, H. Theory on Rates of Excitation-Energy Transfer between Molecular Aggregates through Distributed Transition Dipoles with Application to the Antenna System in Bacterial Photosynthesis. *J. Phys. Chem. B* **1999**, *103*, 252–260.

(30) Knutson, J. R.; Walbridge, D. G.; Brand, L. Decay-associated fluorescence spectra and the heterogeneous emission of alcohol dehydrogenase. *Biochemistry* **1982**, *21*, 4671–4679.

(31) Kimura, A.; Kakitani, T. Theoretical Analysis of the Energy Gap Dependence of the Reconstituted B800 $\rightarrow$ B850 Excitation Energy Transfer Rate in Bacterial LH2 Complexes. *J. Phys. Chem. B* **2003**, *107*, 7932–7939.

(32) Renger, T.; Marcus, R. A. On the relation of protein dynamics and exciton relaxation in pigment–protein complexes: An estimation of the spectral density and a theory for the calculation of optical spectra. *J. Chem. Phys.* **2002**, *116*, 9997–10019.

(33) Renger, T.; Müh, F. Theory of excitonic couplings in dielectric media. Foundation of Poisson-TrEsp method and application to photosystem I trimers. *Photosynth. Res.* **2012**, *111*, 47–52.

(34) Azai, C.; Kim, K.; Kondo, T.; Harada, J.; Itoh, S.; Oh-oka, H. A heterogeneous tag-attachment to the homodimeric type 1 photosynthetic reaction center core protein in the green sulfur bacterium *Chlorobaculum tepidum*. *BBA-Bioenergetics* **2011**, *1807*, 803 – 812.

(35) Oh-oka, H. Type 1 Reaction Center of Photosynthetic Heliobacteria. *Photochem. Photobiol.* **2007**, *83*, 177–186.

(36) Itoh, S.; Mino, H.; Itoh, K.; Shigenaga, T.; Uzumaki, T.; Iwaki, M. Function of chlorophyll d in reaction centers of photosystems I and II of the oxygenic photosynthesis of *Acaryochloris marina*. *Biochemistry* **2007**, *46*, 12472–12481.

Graphical TOC Entry